


 Cite this: *RSC Adv.*, 2023, **13**, 23984

# [Cs@C<sub>18</sub>]<sup>+</sup> and [Na@C<sub>14</sub>]<sup>+</sup>: perfect planar alkaline-metal-centered polyynic cyclo[n]carbon complexes with record coordination numbers†

Min Zhang, Rui-Nan Yuan, Yan-Bo Wu, Qiang Chen, Zhihong Wei and Si-Dian Li \*

Searching for the maximum coordination number (CN) in planar species with novel bonding patterns has fascinated chemists for many years. Using the experimentally observed polyynic cyclo[18]carbon  $D_{9h}$  C<sub>18</sub> and theoretically predicted polyynic cyclo[14]carbon  $D_{7h}$  C<sub>14</sub> as effective ligands and based on extensive first-principles theory calculations, we predict herein their perfect planar alkaline-metal-centered complexes  $D_{9h}$  Cs@C<sub>18</sub><sup>+</sup> (1) and  $D_{7h}$  Na@C<sub>14</sub><sup>+</sup> (4) which as the global minima of the systems possess the record coordination numbers of CN = 18 and 14 in planar polyynic species, respectively. More interestingly, detailed energy decomposition and adaptive natural density partitioning bonding analyses indicate that the hypercoordinate alkaline-metal centers in these complexes exhibit obvious transition metal behaviors, with effective in-plane ( $\pi$ -6s) $\sigma$ , ( $\pi$ -7p) $\sigma$ , and ( $\pi$ -5d) $\sigma$  coordination bonds formed in Cs@C<sub>18</sub><sup>+</sup> (1) and ( $\pi$ -3s) $\sigma$ , ( $\pi$ -3p) $\sigma$ , and ( $\pi$ -3d) $\sigma$  coordination interactions fabricated in Na@C<sub>14</sub><sup>+</sup> (4) to dominate the overall attractive interactions between the metal center and its cyclo[n]carbon ligand. Similarly, alkaline-metal-centered planar  $C_s$  Cs@C<sub>17</sub>B (2),  $C_{2v}$  Cs@C<sub>17</sub><sup>-</sup> (3),  $C_{2v}$  Na@C<sub>13</sub>B (5), and  $C_{2v}$  Na@C<sub>13</sub><sup>-</sup> (6) have also been obtained with CN = 18, 17, 14, and 13, respectively.

Received 12th June 2023

Accepted 4th August 2023

DOI: 10.1039/d3ra03930g

[rsc.li/rsc-advances](http://rsc.li/rsc-advances)

## 1 Introduction

The successive discoveries of fullerenes in 1985,<sup>1</sup> carbon nanotubes in 1991,<sup>2</sup> and graphene in 2004<sup>3</sup> which all consist exclusively of 3-coordinate carbon atoms have sparked a new field of synthetic carbon allotropes in chemistry. The recent characterization of polyynic cyclo[18]carbon  $D_{9h}$  C<sub>18</sub> with bond length alternation (BLA) in 2019 using high-resolution atomic force microscopy marked the onset of an alternative family of molecular carbon allotropes consisting solely of 2-coordinate carbon atoms in the C<sub>4N+2</sub> cyclo[n]carbon ring series.<sup>4</sup> Previous gas-phase experiments indicated that cyclo[n]carbon rings as primary precursors may coalescence to form fullerenes and carbon nanotubes.<sup>5,6</sup> Electronic spectroscopic measurements showed that both C<sub>18</sub> and C<sub>14</sub> possess monocyclic geometries, though these studies did not reveal whether they have cumulantic or polyynic structures.<sup>7,8</sup> High level quantum Monte Carlo (QMC) simulation and coupled cluster methods with single and double excitations (CCSD) investigations indicated that both polyynic  $D_{9h}$  C<sub>18</sub> and  $D_{7h}$  C<sub>14</sub> are the ground states of the systems due to second-order Jahn-Teller effects, with their

cumulantic counterparts with no BLA always behaving as transition states.<sup>9,10</sup> Such perfect monocyclic  $D_{(2N+1)h}$  C<sub>4N+2</sub> polyynic species have aroused considerable interests among chemists and presented viable possibilities to form planar metal-doped cyclo[n]carbon complexes with super-high coordination numbers (CN). A recent theoretical investigation<sup>11</sup> suggested that the Li-doped C<sub>18</sub> complex may serve as a potential optical switch which transforms between two stable  $C_s$  configurations with Li inside (Li@C<sub>18</sub><sup>in</sup>) and outside the carbon ring (Li@C<sub>18</sub><sup>out</sup>). However, in the ground state (Li@C<sub>18</sub><sup>in</sup>) of such an alkaline-metal-doped cyclo[18]carbon complex, the Li atom with the coordination number of CN = 5 appears to be severely off-centered due to the size mismatch between Li and its monocyclic C<sub>18</sub> ligand. Similar situation happens in the recently proposed metal-doped M@C<sub>16</sub> complexes (M = Ca, Sc, Ti, V, Ce, U) in which the off-centered alkaline-earth, lanthanide, or actinide metal atoms have the coordination numbers between CN = 4 ~ 6,<sup>12</sup> again due to size effect. A recent first-principles theory investigation by our group indicated that, in the experimentally observed La@C<sub>13</sub><sup>+</sup>, the La center with the large atomic radius of  $r_{La} = 1.83$  Å<sup>13</sup> matches the C<sub>13</sub> ligand perfectly both geometrically and electronically to form the perfect planar La-centered  $D_{13h}$  La@C<sub>13</sub><sup>+</sup> which has the highest coordination number of CN = 13 in planar species reported to date, demonstrating the unique coordinating capability of cyclo[n]carbon rings as effective ligands to metal centers in chemistry.<sup>14</sup>

Shanxi University, China. E-mail: lisidian@sxu.edu.cn; weizhihong@sxu.edu.cn; chenqiang@sxu.edu.cn

† Electronic supplementary information (ESI) available. See DOI: <https://doi.org/10.1039/d3ra03930g>



However, it still remains unknown to date in both experiments and theory whether or not metal-centered hypercoordinate planar cyclo[n]carbon complexes with  $\text{CN} > 13$  can be achieved in chemistry. To achieve higher CNs ( $\text{CN} = n \geq 14$ ) in metal-centered cyclo[n]carbon complexes, it requires in chemical intuition that the metal centers have atomic radii greater than that of La.

Searching for the maximum coordination number in planar species is more than a curiosity, it is to push the limits and ultimately to understand the essential concepts in chemistry.<sup>14,15</sup> To successfully design a metal-centered hyper-coordinate planar complex, the metal center and its ligand must match both geometrically and electronically, *i.e.*, they must have the right geometrical sizes and electronic configurations. The prototypical electron-deficient planar cyclo[n] boron rings have proven to be effective ligands to coordinate transition metal centers. Perfect  $\sigma + \pi$  dually aromatic wheel-like  $D_{8h}$   $\text{Co}@\text{B}_8^-$ ,  $D_{9h}$   $\text{Ru}@\text{B}_9^-$ ,  $D_{9h}$   $\text{Rh}@\text{B}_9^-$ ,  $D_{9h}$   $\text{Ir}@\text{B}_9^-$ ,  $D_{10h}$   $\text{Ta}@\text{B}_{10}^-$ , and  $D_{10h}$   $\text{Nb}@\text{B}_{10}^-$  with  $\text{CN} = 8, 9, 9, 9, 10$ , and 10 have been observed in gas phases in recent joint photoelectron spectroscopy and first-principles theory investigations.<sup>15-20</sup> These results present the possibility to form metal-centered hyper-coordinate planar complexes using  $\text{C}_n\text{B}_m$  binary monocyclic rings as effective ligands, as indicated in the cases of the previously reported  $C_{2v}$   $\text{Y}@\text{B}_6\text{C}_6^+$  and  $C_{2v}$   $\text{Sc}@\text{B}_5\text{C}_6$ .<sup>14</sup>

Alkaline-earth metal centers in their perfect body-centered cubic carbonyl complexes  $O_h$   $\text{M}(\text{CO})_8^+$  ( $\text{M} = \text{Ca, Sr, or Ba}$ ) in low-temperature neon matrixes have been confirmed to be honorary transition metals with effective  $\text{M}-(\text{CO})_8$  ( $\pi$ ) coordination interactions.<sup>21</sup> Similar  $\text{M}(\text{d}_\pi)-(\text{CO})_8$  ( $\pi$ ) coordination bonds were predicted to exist in  $O_h$   $\text{M}(\text{CO})_8^-$  complexes ( $\text{M} = \text{K, Rb}$ ) in which the alkaline metal centers K and Rb exhibit transition metal behaviours.<sup>22</sup> Given the fact that alkaline metals possess the largest atomic radii in the periodical table<sup>23</sup> and have the potential to form complexes with transition metal behaviors, it is possible to form alkaline-metal-doped cyclo[n] carbon complexes ( $n \geq 14$ ) or their boron-substituted derivatives with  $\text{CN} \geq 14$  if the alkaline metal center and its ligand are chosen properly to match both geometrically and electronically.

Keeping the inspirations in mind, using the experimentally observed perfect planar ring-like  $D_{9h}$   $\text{C}_{18}$  and theoretically predicted  $D_{7h}$   $\text{C}_{14}$  as ligands and based on extensive global minimum searches augmented with first-principles theory calculations, we predict in this work the perfect planar alkaline-metal-centered  $D_{9h}$   $\text{Cs}@\text{C}_{18}^+$  (**1**) and  $D_{7h}$   $\text{Na}@\text{C}_{14}^+$  (**4**) which have the record coordination numbers of  $\text{CN} = 18$  and 14 in planar species, respectively. Cs and Na with the atomic radii of  $r_{\text{Cs}} = 2.65 \text{ \AA}$  and  $r_{\text{Na}} = 1.86 \text{ \AA}$ <sup>13</sup> prove to match the  $D_{9h}$   $\text{C}_{18}$  and  $D_{7h}$   $\text{C}_{14}$  ligands perfectly both geometrically and electronically, respectively. Effective in-plane ( $\pi$ -s) $\sigma$ , ( $\pi$ -p) $\sigma$ , and ( $\pi$ -d) $\sigma$  coordination bonds are formed to dominate the attractive interactions in these novel complexes in which the alkaline-metal centers exhibit transition metal behaviors. The iso-chemical shielding surfaces and out-of-plane  $\pi$  and in-plane  $\sigma$  ring current maps of the concerned species are computationally simulated to evidence their  $\sigma + \pi$  dual aromaticity.

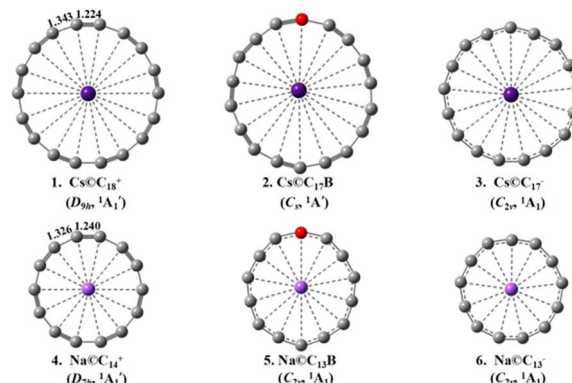


Fig. 1 Optimized structures of  $D_{9h}$   $\text{Cs}@\text{C}_{18}^+$  (**1**),  $C_s$   $\text{Cs}@\text{C}_{17}\text{B}$  (**2**),  $C_{2v}$   $\text{Cs}@\text{C}_{17}^-$  (**3**),  $D_{7h}$   $\text{Na}@\text{C}_{14}^+$  (**4**),  $C_{2v}$   $\text{Na}@\text{C}_{13}\text{B}$  (**5**), and  $C_{2v}$   $\text{Na}@\text{C}_{13}^-$  (**6**) at M06-2X level.

## 2 Computational details

Extensive global-minimum (GM) searches were performed on  $\text{Cs}@\text{C}_{18}^+$ ,  $\text{Na}@\text{C}_{14}^+$ ,  $\text{Cs}@\text{C}_{17}\text{B}$ ,  $\text{Cs}@\text{C}_{17}^-$ ,  $\text{Na}@\text{C}_{13}\text{B}$ , and  $\text{Na}@\text{C}_{13}^-$  using the TGmin2 code<sup>24</sup> at DFT level based on the basin-hopping algorithm.<sup>25</sup> Over 1000 stationary points were explored for each species at PBE/DZVP level employing the CP2K program.<sup>26,27</sup> The low-lying isomers were then fully optimized at both M06-2X and  $\omega$ B97XD levels<sup>28,29</sup> with vibrational frequencies checked, with the aug-cc-pvtz basis set for C, B, Na, and K and Stuttgart relativistic small-core pseudopotentials<sup>30,31</sup> for Rb, Cs, and Fr, using the Gaussian16 program.<sup>32</sup> The fact that M06-2X produces essentially the same polyynic  $D_{9h}$   $\text{C}_{18}$  and  $D_{7h}$   $\text{C}_{14}$  structures (Fig. S1†) as that obtained at the more accurate QMC and CCSD levels<sup>9,10</sup> evidences the reliability of the optimized geometries depicted in Fig. 1. Natural bond orbital (NBO) analyses were performed using NBO 7.0 program.<sup>33</sup> The energy decomposition analyses (EDA) together with the natural orbitals for chemical valence (NOCV) calculations, denoted as EDA-NOCV,<sup>34-36</sup> were carried out with the ADF program package<sup>37</sup> at M06-2X/TZ2P<sup>38</sup> level where scalar relativistic effects were considered for Cs using the zero order regular approximation (ZORA).<sup>39</sup> The frozen core approximation was not employed in EDA-NOCV computations. The overall interaction energy ( $\Delta E_{\text{int}}$ ) between two fragments is divided into three main terms: the electrostatic interaction energy ( $\Delta E_{\text{elstat}}$ ), Pauli repulsion ( $\Delta E_{\text{Pauli}}$ ), and orbital interaction energy ( $\Delta E_{\text{orb}}$ ) in eqn (1):

$$\Delta E_{\text{int}} = \Delta E_{\text{elstat}} + \Delta E_{\text{Pauli}} + \Delta E_{\text{orb}}. \quad (1)$$

Detailed bonding analyses on  $D_{9h}$   $\text{Cs}@\text{C}_{18}^+$  (**1**),  $D_{7h}$   $\text{Na}@\text{C}_{14}^+$  (**4**), and  $C_s$   $\text{Cs}@\text{C}_{17}\text{B}$  (**2**) were implemented using the adaptive natural density partitioning (AdNDP 2.0) approach<sup>40,41</sup> at the M06-2X/6-31G level, with the isosurface maps of the orbitals visualized using the Visual Molecular Dynamics (VMD) software.<sup>42</sup> The iso-chemical shielding surfaces (ICSSs)<sup>43,44</sup> and isosurfaces of localized orbital locators (LOL)<sup>45</sup> were obtained with Multiwfn 3.8 code.<sup>46</sup> The anisotropy of the current-induced



density (ACID) analyses were realized by the ACID code,<sup>47</sup> with the maps finally generated by POV-Ray render.<sup>48</sup>

## 3 Results and discussions

### 3.1 Structures and stabilities

The optimized GM structures of  $D_{9h}$   $\text{Cs}\text{C}_{18}^+$  (1),  $C_s$   $\text{Cs}\text{C}_{17}\text{B}$  (2),  $C_{2v}$   $\text{Cs}\text{C}_{17}^-$  (3),  $D_{7h}$   $\text{Na}\text{C}_{14}^+$  (4),  $C_{2v}$   $\text{Na}\text{C}_{13}\text{B}$  (5), and  $C_{2v}$   $\text{Na}\text{C}_{13}^-$  (6) are collectively plotted in Fig. 1, with more alternative isomers summarized in Fig. S3–S8.† Fig. S2† depicts the optimized GM structures of (a) the alkaline-metal-centered cyclo[18]carbon complexes  $\text{M}\text{C}_{18}^+$  with  $\text{M} = \text{Li}, \text{Na}, \text{K}, \text{Rb}, \text{Cs}$ , and  $\text{Fr}$  and (b) alkaline-metal-centered cyclo[14]carbon complexes  $\text{M}\text{C}_{14}^+$  with  $\text{M} = \text{Li}, \text{Na}$ , and  $\text{K}$  at M06-2X. It is noticed that the alkaline metal atoms in the GMs are all located inside the cyclo[n]carbon rings, with the alkaline metal atoms severely off-centered in  $C_{2v}$   $\text{Li}\text{C}_{18}^+$ ,  $C_{2v}$   $\text{Na}\text{C}_{18}^+$ ,  $C_{2v}$   $\text{K}\text{C}_{18}^+$ , and  $C_{2v}$   $\text{Li}\text{C}_{14}^+$  and slightly off-centered in  $C_s$   $\text{Rb}\text{C}_{18}^+$  and  $C_s$   $\text{Fr}\text{C}_{18}^+$ . The  $\text{K}$  atom in  $C_{7v}$   $\text{K}\text{C}_{14}^+$  lies about 1.14 Å above the ligand plane along the  $C_7$  molecular axis due to its large atomic radius ( $r_{\text{K}} = 2.32$  Å) which appears to be too big to be hosted inside the  $\text{C}_{14}$  ring.

Encouragingly, the  $\text{Cs}$  center with the NBO net atomic charge of  $q_{\text{Cs}} = +0.99 |e|$  proves to have the right atomic radius of  $r_{\text{Cs}} = 2.65$  Å to be coordinated exactly at the center of the  $D_{9h}$   $\text{C}_{18}$  ligand in  $D_{9h}$   $\text{Cs}\text{C}_{18}^+$  (1) to achieve the highest coordination number of  $\text{CN} = 18$  reported to date. As the well-defined GM of the complex (Fig. S3†),  $\text{Cs}\text{C}_{18}^+$  (1) exhibits the alternating bond lengths of  $r_{\text{C}-\text{C}} = 1.343$  Å and  $r_{\text{C}\equiv\text{C}} = 1.224$  Å at M06-2X which are well inherited from its parent ligand  $D_{9h}$   $\text{C}_{18}$  ligand with  $r_{\text{C}-\text{C}} = 1.343$  Å and  $r_{\text{C}\equiv\text{C}} = 1.223$  Å at the same theoretical level (Fig. S1 and Table S1†).

The large calculated HOMO–LUMO gap of  $\Delta E_{\text{gap}} = 5.38$  eV at M06-2X well supports its high chemical stability. The second isomer  $C_{2v}$   $\text{Cs}\text{C}_{18}^+$  with a  $\text{Cs}^+$  located outside the  $\text{C}_{18}$  ring and the seventh isomer  $C_{2v}$   $\text{Cs}\text{C}_{18}^+$  with a  $\text{Cs}^+$  inserted into the  $\text{C}_{18}$  ring appear to be 0.38 eV and 4.79 eV less stable than  $D_{9h}$  GM at M06-2X, respectively (Fig. S3†). The slightly off-centered planar  $C_s$   $\text{Rb}\text{C}_{18}^+$  and  $C_s$   $\text{Fr}\text{C}_{18}^+$  also possess the coordination numbers of  $\text{CN} = 18$  (Fig. S2†). Both the planar neutral  $C_s$   $\text{Cs}\text{C}_{17}\text{B}$  (2) which is isoelectronic with  $\text{Cs}\text{C}_{18}^+$  (1) with obviously bond-length alternations and  $C_{2v}$   $\text{Cs}\text{C}_{17}^-$  (3) with roughly the same averaged bond lengths are the well-defined GMs of the systems with  $\text{CN} = 18$  and 17, respectively (Fig. S4 and S5†). However, the severely off-centered  $C_{2v}$   $\text{Li}\text{C}_{18}^+$ ,  $C_{2v}$   $\text{Na}\text{C}_{18}^+$ , and  $C_{2v}$   $\text{K}\text{C}_{18}^+$  with obvious smaller alkaline metal centers  $\text{Li}, \text{Na}$ , and  $\text{K}$  appear to have much smaller coordination numbers with  $\text{CN} = 4 \sim 6$  (Fig. S2†).

Similarly, the  $\text{Na}$  center with  $q_{\text{Na}} = +0.95 |e|$  appears to have the right atomic radius ( $r_{\text{Na}} = 1.86$  Å) to be hosted exactly at the center of the  $D_{7h}$   $\text{C}_{14}$  ligand to form the perfect planar polyytic  $D_{7h}$   $\text{Na}\text{C}_{14}^+$  (4) (Fig. S6†) with  $\text{CN} = 14$ . The second lowest-lying isomer  $C_s$   $\text{Na}\text{C}_{14}^+$  with the  $\text{Na}^+$  center located outside the  $\text{C}_{14}$  ring lies only 0.23 eV higher than  $\text{Na}\text{C}_{14}^+$  (4) (Fig. S6†). The two close-lying lowest-lying isomers of  $\text{Cs}\text{C}_{18}^+$  and  $\text{Na}\text{C}_{14}^+$  discussed above (Fig. S3 and S6†) may transform between each other with low energy barriers under certain conditions.

$\text{Na}\text{C}_{14}^+$  (4) as the GM of the system has the alternating bond lengths of  $r_{\text{C}-\text{C}} = 1.326$  Å and  $r_{\text{C}\equiv\text{C}} = 1.240$  Å at M06-2X well comparable with the corresponding values of  $r_{\text{C}-\text{C}} = 1.324$  Å and  $r_{\text{C}\equiv\text{C}} = 1.237$  Å calculated for  $D_{7h}$   $\text{C}_{14}$  at the same theoretical level (Fig. S1 and Table S1†), while  $\text{Li}$  with the atomic radius of  $r_{\text{Li}} = 1.52$  Å proves to be too small and  $\text{K}$  with  $r_{\text{K}} = 2.32$  Å appears to be too big to be hosted at the ring center of the  $\text{C}_{14}$  ligand, they form severely off-centered and off-planed structures, respectively (Fig. S2†). With the HOMO–LUMO gap of  $\Delta E_{\text{gap}} = 5.87$  eV,  $\text{Na}\text{C}_{14}^+$  (4) is expected to have a high chemical stability. The slightly off-centered planar  $C_{2v}$   $\text{Na}\text{C}_{13}\text{B}$  (5) with  $\text{CN} = 14$  and vibrationally averaged  $C_{2v}$   $\text{Na}\text{C}_{13}^-$  (6) with  $\text{CN} = 13$  with roughly the averaged bond lengths also appear to be the well-defined GMs of the systems (Fig. S7 and S8†).

As expected, the high-symmetry  $\text{Cs}\text{C}_{18}^+$  (1) and  $\text{Na}\text{C}_{14}^+$  (4) exhibit highly characteristic calculated vibrational spectroscopic features as shown in their simulated IR spectra in Fig. S9,† with the former possessing well characterized IR peaks at 513 and 2202  $\text{cm}^{-1}$  and Raman active vibrations at 1792 and 2293  $\text{cm}^{-1}$ , respectively, while the latter having two well separated IR peaks at 545 and 2160  $\text{cm}^{-1}$  and one dominant Raman feature at 1252  $\text{cm}^{-1}$ . Such well-defined spectral features can help facilitate future experimental characterizations of these species. Their simulated UV-vis spectra are also shown in Fig. S9† with 100 excited states included to better understand their electronic structures.

### 3.2 EDA-NOCV bonding scheme analyses

To shed insights into the bonding nature of  $D_{9h}$   $\text{Cs}\text{C}_{18}^+$  (1) and  $D_{7h}$   $\text{Na}\text{C}_{14}^+$  (4), detailed EDA-NOCV analyses were carried out at M06-2X/TZ2P. The  $D_{3h}$  subgroup was applied to  $D_{9h}$   $\text{Cs}\text{C}_{18}^+$  (1) because the highest point group supported by ADF program is  $D_{8h}$ . It was found that  $\text{Cs}^+$  and  $\text{C}_{18}$  as the most possible reacting fragments give the most favourite orbital interaction energy of  $\Delta E_{\text{orb}} = -13.95$  kcal mol<sup>-1</sup> for  $\text{Cs}\text{C}_{18}^+$  (1) in different fragmental schemes (Table S2†). They are thus chosen as interacting species to demonstrate the bonding scheme of  $\text{Cs}\text{C}_{18}^+$  (1) in Fig. 2(a). Similarly,  $\text{Na}^+$  and  $\text{C}_{14}$  as reacting fragments with  $\Delta E_{\text{orb}} = -22.41$  kcal mol<sup>-1</sup> are chosen for  $\text{Na}\text{C}_{14}^+$  (4) in Fig. 2(b).

The bonding molecular orbitals (MOs)  $15a_1'$ ,  $19e_1'$  and  $20e_1'$  of  $D_{3h}$   $\text{Cs}\text{C}_{18}^+$  representing covalent bonding MOs between  $\text{Cs}^+$  and  $\text{C}_{18}$  are connected with the corresponding fragmental orbitals by bold dashed lines in Fig. 2(a), with the orbital compositions tabulated in Table S3.† The non-degenerate  $15a_1'$  mainly originates from the occupied  $8a_1'$  of  $\text{C}_{18}$  with in-plane  $\pi$  characteristics (abbreviated as  $\pi_{\text{in}}$ ) and vacant 6s of  $\text{Cs}^+$  via ( $\pi$ -6s) $\sigma$  coordination interaction, the doubly degenerate  $19e_1'$  is composed of the occupied in-plane  $13e_1'$  ( $\pi_{\text{in}}$ ) of  $\text{C}_{18}$  with one nodal plane and vacant  $7p_x$  and  $7p_y$  of  $\text{Cs}^+$  via ( $\pi$ -7p) $\sigma$  coordination, while the doubly degenerate  $20e_1'$  is composed of the occupied  $14e_1'$  of  $\text{C}_{18}$  with  $\pi_{\text{in}}$  characteristics with two nodal planes and vacant  $5d_{xy}$  and  $5d_{x^2-y^2}$  of  $\text{Cs}^+$  via ( $\pi$ -5d) $\sigma$  coordination. As detailed in Table 1, EDA analyses demonstrate that the overall interaction energy of  $\Delta E_{\text{int}} = -15.22$  kcal mol<sup>-1</sup> between the  $\text{Cs}^+$  and  $\text{C}_{18}$  in  $\text{Cs}\text{C}_{18}^+$  consists of the Pauli repulsion



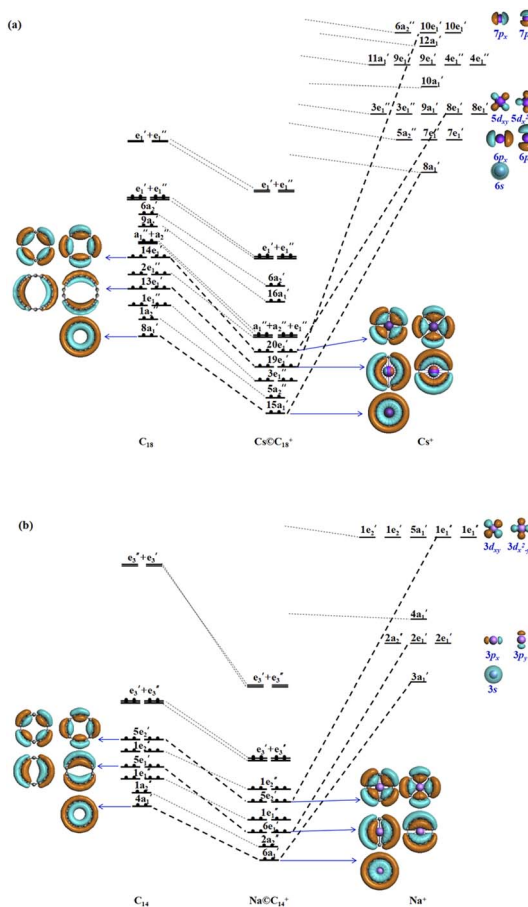


Fig. 2 (a) MO bonding scheme of  $D_{3h}$   $\text{Cs}@\text{C}_{18}^+$  with the fragments of  $\text{C}_{18}$  and  $\text{Cs}^+$  as interacting species and (b) MO bonding scheme of  $D_{7h}$   $\text{Na}@\text{C}_{14}^+$  with  $\text{C}_{14}$  and  $\text{Na}^+$  as interacting species at M06-2X/TZ2P-ZORA level.

$\Delta E_{\text{Pauli}} = 1.89 \text{ kcal mol}^{-1}$ , coulombic attraction  $\Delta E_{\text{elstat}} = -3.16 \text{ kcal mol}^{-1}$ , and orbital interaction  $\Delta E_{\text{orb}} = -13.95 \text{ kcal mol}^{-1}$ , with covalent orbital interaction making a dominating contribution of 81.5% to the overall attraction interaction ( $-17.11 \text{ kcal mol}^{-1}$ ), while electrostatic attraction contributing only 18.5%. The decompositions of the orbital interactions  $\Delta E_{\text{orb}}$  into pairwise contributions between occupied and vacant MOs of the fragments provide quantitative

insight into the charge flow. The strongest orbital interaction  $\Delta E_{\text{orb}(1)}$  (20e<sub>1'</sub>, 27.5%) arises mainly from  $[\text{C}_{18}(\pi_{\text{in}})] \rightarrow [\text{Cs}^+(5d)]$  where  $\text{C}_{18}$  serves as a  $\pi_{\text{in}}$ -donor to coordinate the 5d<sub>xy</sub> and 5d<sub>x<sup>2</sup>-y<sup>2</sup></sub> orbitals of the  $\text{Cs}^+$  as  $\sigma$ -acceptors. The orbital interaction  $\Delta E_{\text{orb}(2)}$  (19e<sub>1'</sub>, 16.8%) originates from  $[\text{C}_{18}(\pi_{\text{in}})] \rightarrow [\text{Cs}^+(7p)]$  where the 7p<sub>x</sub> and 7p<sub>y</sub> orbitals of the  $\text{Cs}^+$  serve as  $\sigma$ -acceptors. The orbital interaction  $\Delta E_{\text{orb}(3)}$  (15a<sub>1'</sub>, 14.1%) originates from  $[\text{C}_{18}(\pi_{\text{in}})] \rightarrow [\text{Cs}^+(6s)]$  where the 6s orbital of the  $\text{Cs}^+$  is a  $\sigma$ -acceptor. Fig. S10<sup>†</sup> shows the corresponding deformation densities  $\Delta\rho$  associated with the pairwise interactions  $\Delta E_{\text{orb}(1)}$ ,  $\Delta E_{\text{orb}(2)}$  and  $\Delta E_{\text{orb}(3)}$  in  $\text{Cs}@\text{C}_{18}^+$ , further indicating that  $\text{C}_{18}$  serves as a  $\pi_{\text{in}}$ -donor while  $\text{Cs}^+$  is a  $\sigma$ -acceptor in the complex.

Detailed EDA-NOCV calculations for  $D_{7h}$   $\text{Na}@\text{C}_{14}^+$  (4) gives a similar trend as shown in Fig. 2(b) and Table 1. The bonding MOs 6a<sub>1'</sub>, 6e<sub>1'</sub> and 5e<sub>2'</sub> representing covalent bonding interactions between the  $\text{Na}^+$  and  $\text{C}_{14}$  fragmental orbitals are connected by bold dashed lines, with the orbital compositions listed in Table S4.<sup>†</sup> The 6a<sub>1'</sub> mainly originates from the occupied 4a<sub>1'</sub> of  $\text{C}_{14}$  with  $\pi_{\text{in}}$  characteristics and vacant 3s of  $\text{Na}^+$  via  $(\pi\text{-}3s)\sigma$  coordination interaction, the doubly degenerate 6e<sub>1'</sub> is composed of occupied 5e<sub>1'</sub> of  $\text{C}_{14}$  with  $\pi_{\text{in}}$  characteristics and vacant 3p<sub>x</sub> and 3p<sub>y</sub> of  $\text{Na}^+$  via  $(\pi\text{-}3p)\sigma$  coordination, while the 5e<sub>2'</sub> is composed of  $\text{C}_{14}$  with  $\pi_{\text{in}}$  characteristics and vacant 3d<sub>xy</sub> and 3d<sub>x<sup>2</sup>-y<sup>2</sup></sub> of  $\text{Na}^+$  via  $(\pi\text{-}3d)\sigma$  coordination.

EDA analyses (Table 1) indicate that overall attraction interaction is overwhelmingly dominated by covalent orbital contribution (94.0%), while electrostatic attraction makes only a marginal contribution (6.0%). The decompositions of  $\Delta E_{\text{orb}}$  into pairwise contributions between occupied and vacant MOs of the fragments reveals that the strongest orbital interaction  $\Delta E_{\text{orb}(1)}$  (24.9%) originates mainly from  $[\text{C}_{14}(\pi_{\text{in}})] \rightarrow [\text{Na}^+(3p)]$ , the orbital interaction  $\Delta E_{\text{orb}(2)}$  (19.2%) arises mainly from  $[\text{C}_{14}(\pi_{\text{in}})] \rightarrow [\text{Na}^+(3s)]$ , while the orbital interaction  $\Delta E_{\text{orb}(3)}$  (18.1%) originates from  $[\text{C}_{14}(\pi_{\text{in}})] \rightarrow [\text{Na}^+(3d)]$ . The corresponding deformation densities  $\Delta\rho$  associated with the pairwise interactions  $\Delta E_{\text{orb}(1)}$ ,  $\Delta E_{\text{orb}(2)}$  and  $\Delta E_{\text{orb}(3)}$  in  $\text{Na}@\text{C}_{14}^+$  in Fig. S11<sup>†</sup> clearly indicate that  $\text{C}_{14}$  serves as a  $\pi_{\text{in}}$ -donor while  $\text{Na}^+$  is a  $\sigma$ -acceptor.

The EDA-NOCV results detailed above quantitatively indicate that the cyclo[4N+2]carbon ligands ( $N = 4, 3$ ) serve as good  $\pi_{\text{in}}$ -donors to stabilize alkaline metal centers in both  $\text{Cs}@\text{C}_{18}^+$  (1) and  $\text{Na}@\text{C}_{14}^+$  (4) by donating their  $\pi_{\text{in}}$  valence electrons partially

Table 1 EDA-NOCV results for  $\text{Cs}@\text{C}_{18}^+$  (1) and  $\text{Na}@\text{C}_{14}^+$  (4) at the M06-2X/TZ2P-ZORA level, taking  $\text{C}_{18}$  with  $\text{Cs}^+$  and  $\text{C}_{14}$  with  $\text{Na}^+$  as interacting fragments, respectively. Energy values are given in kcal mol<sup>-1</sup>

Energy terms	Interaction	$\text{Cs}^+ + \text{C}_{18}$	Interaction	$\text{Na}^+ + \text{C}_{14}$
$\Delta E_{\text{int}}$		-15.22		-24.44
$\Delta E_{\text{elstat}}^a$		-3.16 (18.5%)		-1.42 (6.0%)
$\Delta E_{\text{Pauli}}$		1.89		3.45
$\Delta E_{\text{orb}}^a$		-13.95 (81.5%)		-22.41 (94.0%)
$\Delta E_{\text{orb}(1)}^b$	$\text{C}_{18}(\pi_{\text{in}})$ donation $\rightarrow [\text{Cs}^+(5d)]$	-3.84 (27.5%)	$\text{C}_{14}(\pi_{\text{in}})$ donation $\rightarrow [\text{Na}^+(3p)]$	-5.58 (24.9%)
$\Delta E_{\text{orb}(2)}^b$	$\text{C}_{18}(\pi_{\text{in}})$ donation $\rightarrow [\text{Cs}^+(7p)]$	-2.34 (16.8%)	$\text{C}_{14}(\pi_{\text{in}})$ donation $\rightarrow [\text{Na}^+(3s)]$	-4.30 (19.2%)
$\Delta E_{\text{orb}(3)}^b$	$\text{C}_{18}(\pi_{\text{in}})$ donation $\rightarrow [\text{Cs}^+(6s)]$	-1.96 (14.1%)	$\text{C}_{14}(\pi_{\text{in}})$ donation $\rightarrow [\text{Na}^+(3d)]$	-4.06 (18.1%)
$\Delta E_{\text{orb(rest)}}$ <sup>b</sup>		-5.81 (41.6%)		-8.47 (37.8%)

<sup>a</sup> The value in parentheses gives the percentage contribution to the total attractive interactions ( $\Delta E_{\text{elstat}} + \Delta E_{\text{orb}}$ ). <sup>b</sup> The value in parentheses gives the percentage contribution to the total orbital interaction ( $\Delta E_{\text{orb}}$ ).



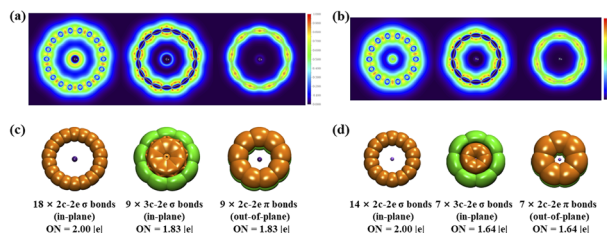


Fig. 3 Color-filled maps of the localized orbital locator isosurfaces of (a)  $D_{9h}$   $\text{Cs}@\text{C}_{18}^+$  (1) and (b)  $D_{7h}$   $\text{Na}@\text{C}_{14}^+$  (4) and AdNDP bonding patterns of (c)  $D_{9h}$   $\text{Cs}@\text{C}_{18}^+$  (1) and (d)  $D_{7h}$   $\text{Na}@\text{C}_{14}^+$  (4) with the occupation numbers (ON) indicated.

to the vacant s, p, and d orbitals of  $\text{Cs}^+$  and  $\text{Na}^+$  through effective in-plane ( $\pi\text{-s}$ ) $\sigma$ , ( $\pi\text{-p}$ ) $\sigma$ , and ( $\pi\text{-d}$ ) $\sigma$  coordination interactions.

Localized orbital locator (LOL) is an effective space function in revealing the distributions of delocalized electrons on conjugated rings in molecules. We calculated in-plane LOL- $\sigma$ , in-plane LOL- $\pi_{in}$ , and out-of-plane LOL- $\pi_{out}$  separately based on the corresponding in-plane  $\sigma$  MOs, in-plane  $\pi$  MOs, and out-of-plane  $\pi$  MOs of the systems, respectively. To better reflect spatial distributions of LOL- $\sigma$ , LOL- $\pi_{in}$ , and LOL- $\pi_{out}$  in  $\text{Cs}@\text{C}_{18}^+$  (1) and  $\text{Na}@\text{C}_{14}^+$  (4), the color-filled maps of LOL- $\sigma$  on the ring plane, LOL- $\pi_{in}$  on the ring plane, and LOL- $\pi_{out}$  1 Å above the ring plane are plotted in Fig. 3(a) and (b) comparatively. By comparing the area colors on the maps, it can be clearly seen that both LOL- $\pi_{in}$  and LOL- $\pi_{out}$  exhibit heavy density distributions over the short  $\text{C}\equiv\text{C}$  bonds and light density distributions over the long  $\text{C}-\text{C}$  bonds, well supporting the alternating of triple and single bonds in different bond lengths in both polymeric  $\text{Cs}@\text{C}_{18}^+$  (1) and  $\text{Na}@\text{C}_{14}^+$  (4).

### 3.3 AdNDP bonding pattern analyses

Detailed AdNDP analyses in Fig. 3(c) and (d) unveil both the localized and delocalized bonds in  $D_{9h}$   $\text{Cs}@\text{C}_{18}^+$  (1) and  $D_{7h}$   $\text{Na}@\text{C}_{14}^+$  (4) more vividly. As expected, out of the 72 valence

electrons in  $\text{Cs}@\text{C}_{18}^+$  (1), 36 electrons form 18 equivalent 2c-2e C-C peripheral in-plane  $\sigma$  bonds with the occupation numbers of  $\text{ON} = 2.00 \text{ }|e|$ . The remaining 36 valence electrons are distributed in two types of chemical bonds, including 9 equivalent in-plane 3c-2e  $\sigma$  bonds on nine  $\text{CsC}_2$  triangles with  $\text{ON} = 1.83 \text{ }|e|$  and 9 equivalent out-of-plane 2c-2e C-C  $\pi$  bonds with  $\text{ON} = 1.83 \text{ }|e|$ , respectively. Such a bonding pattern follows the  $4N + 2$  aromatic rule for  $\sigma$  aromaticity with  $N_\sigma = 4$  and  $\pi$  aromaticity with  $N_\pi = 4$ , respectively, making the planar complex  $\sigma + \pi$  dually aromatic in nature and rendering extra stability to the system, similar to the situation in the previously reported  $D_{9h}$   $\text{C}_{18}$ .<sup>11</sup>

Similarly, as shown in Fig. 3(d),  $D_{7h}$   $\text{Na}@\text{C}_{14}^+$  (4) possesses 7 equivalent 2c-2e C-C periphery in-plane  $\sigma$  bonds, 7 equivalent 3c-2e in-plane  $\sigma$  bonds on seven  $\text{NaC}_2$  triangles, and 7 equivalent 2c-2e out-of-plane C-C  $\pi$  electrons, again following the  $4N + 2$  aromatic rule with  $N_\sigma = N_\pi = 3$  for  $\sigma + \pi$  dual aromaticity. Similar bonding patterns exist in  $\text{Cs}@\text{C}_{17}\text{B}$  (2) (Fig. S12†). The dual aromaticities of both  $\text{Cs}@\text{C}_{18}^+$  (1) and  $\text{Na}@\text{C}_{14}^+$  (4) are also well supported by numbers of their delocalized in-plane  $\sigma$  MOs and delocalized out-of-plane  $\pi$  MOs shown in Fig. S13.†

The simulated ICSS isosurfaces of  $D_{9h}$   $\text{Cs}@\text{C}_{18}^+$  (1) and  $D_{7h}$   $\text{Na}@\text{C}_{14}^+$  (4) based on the ZZ components of the calculated nuclear-independent chemical shifts (NICS-ZZ) are presented as Fig. 4(a), in comparison with that of the previously reported  $\sigma + \pi$  dually aromatic  $D_{9h}$   $\text{C}_{18}$  and  $D_{7h}$   $\text{C}_{14}$ . It can be clearly seen that, similar to  $D_{9h}$   $\text{C}_{18}$  and  $D_{7h}$   $\text{C}_{14}$ , both  $D_{9h}$   $\text{Cs}@\text{C}_{18}^+$  (1) and  $D_{7h}$   $\text{Na}@\text{C}_{14}^+$  (4) are aromatic in nature, with the spaces inside the cyclo[n]carbon rings and within ~1.0 Å above the ring planes belonging to chemical shielding areas with negative NICS-ZZ values (highlighted in yellow) and the blet-like regions around the cyclo[n]carbon rings in horizontal direction belonging to chemical deshielding areas with positive NICS-ZZ values (highlighted in green).

The widely used ACID method can be employed to display graphically the ring currents induced by an external magnetic

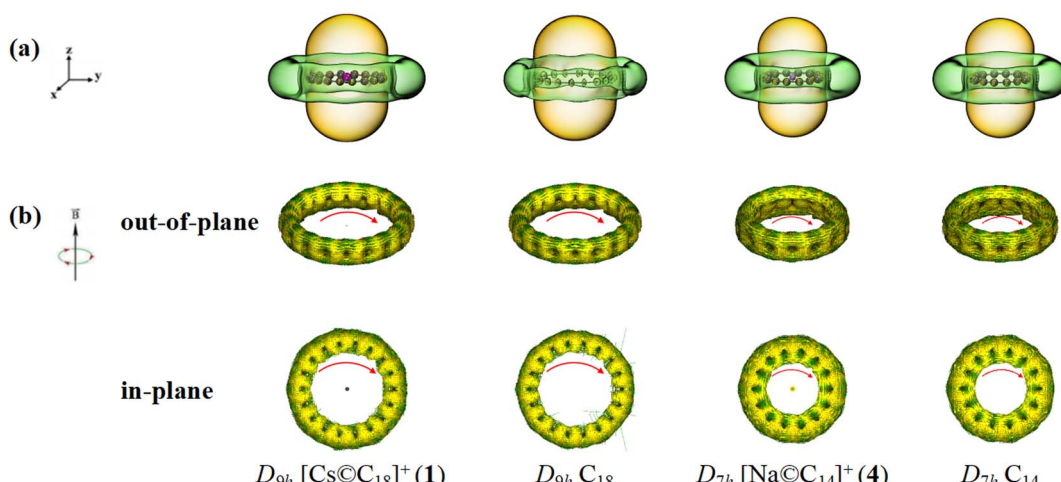


Fig. 4 (a) Calculated iso-chemical shielding surfaces (ICSSs) of  $D_{9h}$   $\text{Cs}@\text{C}_{18}^+$  (1),  $D_{9h}$   $\text{C}_{18}$ ,  $D_{7h}$   $\text{Na}@\text{C}_{14}^+$  (4), and  $D_{7h}$   $\text{C}_{14}$ . Yellow and green regions stand for chemical shielding and deshielding areas, respectively. (b) Calculated out-of-plane- $\pi$  and in-plane- $\sigma$  ring current maps of  $D_{9h}$   $\text{Cs}@\text{C}_{18}^+$  (1) and  $D_{7h}$   $\text{Na}@\text{C}_{14}^+$  (4), compared with the corresponding ring current maps of  $D_{9h}$   $\text{C}_{18}$  and  $D_{7h}$   $\text{C}_{14}$ , respectively. The external magnetic field is perpendicular to the ring plane. The red arrows indicate the directions of the ring currents on the ACID iso-surfaces.



field in vertical directions perpendicular to the cyclo[n]carbon ring. Fig. 4(b) presents the calculated out-of-plane  $\pi$  and in-plane  $\sigma$  ring currents maps for both  $D_{9h}$   $\text{Cs}\text{C}_{18}^+$  (1) and  $D_{7h}$   $\text{Na}\text{C}_{14}^+$  (4), in comparison with the corresponding ring currents obtained for  $D_{9h}$   $\text{C}_{18}$  and  $D_{7h}$   $\text{C}_{14}$  at the same theoretical level, respectively. As clearly indicated in Fig. 4(b), these alkaline-metal-centered polynic complex monocations do possess intrinsic  $\sigma$  aromaticity and  $\pi$  aromaticity simultaneously, similar to their neutral parent ligands  $D_{9h}$   $\text{C}_{18}$  and  $D_{7h}$   $\text{C}_{14}$  in ring current distributions.

## 4 Conclusions

In summary, based on extensive first-principles theory calculations, we have predicted in this work a series of alkaline-metal-centered perfect planar complexes  $\text{Cs}\text{C}_{18}^+$  (1),  $\text{Cs}\text{C}_{17}\text{B}$  (2),  $\text{Cs}\text{C}_{17}^-$  (3),  $\text{Na}\text{C}_{14}^+$  (4),  $\text{Na}\text{C}_{13}\text{B}$  (5), and  $\text{Na}\text{C}_{13}^-$  (6) which turn out to be GMs of the systems with the record coordination numbers of  $\text{CN} = 18 \sim 13$  in planar species. These hyper-coordinate planar complexes possess effective in-plane ( $\pi$ -s) $\sigma$ , ( $\pi$ -p) $\sigma$ , and ( $\pi$ -d) $\sigma$  coordination interactions which dominate the attractive interaction between the alkaline metal center as  $\sigma$ -acceptor and its cyclo[n]carbon ligand as in-plane  $\pi$ -donor, evidencing the transition metal behaviors of the alkaline metal centers in them. Similar to the situation in the recently observed alkaline-earth metal carbonyl species,<sup>21</sup> the proposed perfect planar alkaline-metal-centered polynic  $D_{(2N+1)h}$  cyclo[4N + 2] carbon complexes with relatively low coordination energies may be produced in gas phases by laser ablation of alkaline-metal-carbon mixed binary targets and characterized by spectroscopic measurements at low temperatures to further push the boundary of coordination chemistry.

## Author contributions

S. D. Li, Z. H. Wei, and Q. Chen conceived the project and finalized the manuscript. M. Z. and R. N. Y. did the calculations and prepared the first draft. Y. B. Wu helped analyze the data. All authors approved the final version.

## Conflicts of interest

There are no conflicts to declare.

## Acknowledgements

The work was supported by the National Natural Science Foundation of China (21973057, 21720102006 and 22003034) and Natural Science Foundation of Shanxi Province of China (20210302124002).

## Notes and references

- 1 H. W. Kroto, J. R. Heath, S. C. O'Brien, R. F. Curl and R. E. Smalley, *Nature*, 1985, **318**, 162–163.
- 2 S. Iijima and T. Ichihashi, *Nature*, 1993, **363**, 603–605.

- 3 K. S. Novoselov, A. K. Geim, S. V. Morozov, D. Jiang, Y. Zhang, S. V. Dubonos, I. V. Grigorieva and A. A. Firsov, *Science*, 2004, **306**, 666–669.
- 4 K. Kaiser, L. M. Scriven, F. Schulz, P. Gawel, L. Gross and H. L. Anderson, *Science*, 2019, **365**, 1299–1301.
- 5 G. von Helden, N. G. Gotts and M. T. Bowers, *Nature*, 1993, **363**, 60–63.
- 6 Y. Rubin, M. Kahr, C. B. Knobler, F. Diederich and C. L. Wilkins, *J. Am. Chem. Soc.*, 1991, **113**, 495–500.
- 7 A. E. Boguslavskiy, H. Ding and J. P. Maier, *J. Chem. Phys.*, 2005, **123**, 034305.
- 8 A. E. Boguslavskiy and J. P. Maier, *Phys. Chem. Chem. Phys.*, 2007, **9**, 127–130.
- 9 T. Torelli and L. Mitas, *Phys. Rev. Lett.*, 2000, **85**, 1702–1705.
- 10 S. Arulmozhiraja and T. Ohno, *J. Chem. Phys.*, 2008, **128**, 114301.
- 11 Z. y. Liu, X. Wang, T. Lu, A. h. Yuan and X. f. Yan, *Carbon*, 2022, **187**, 78–85.
- 12 Y. h. Jiang, Y. b. Wu, J. j. Deng and Z. y Wang, *Phys. Chem. Chem. Phys.*, 2021, **23**, 8817–8824.
- 13 J. A. Dean, *Lange's Handbook of Chemistry*, McGraw-Hill Book Co., 15th edn, 1999.
- 14 X. Q. Lu, H. G. Lu and S. D. Li, *RSC Adv.*, 2021, **11**, 27193–27198.
- 15 T. Heine and G. Merino, *Angew. Chem., Int. Ed.*, 2012, **51**, 4275–4276.
- 16 T. R. Galeev, C. Romanescu, W. L. Li, L. S. Wang and A. I. Boldyrev, *Angew. Chem., Int. Ed.*, 2012, **51**, 2101–2105.
- 17 C. Romanescu, T. R. Galeev, W. L. Li, A. I. Boldyrev and L. S. Wang, *Angew. Chem., Int. Ed.*, 2011, **50**, 9334–9337.
- 18 C. Romanescu, T. R. Galeev, W. L. Li, A. I. Boldyrev and L. S. Wang, *J. Chem. Phys.*, 2013, **138**, 134315.
- 19 W. L. Li, C. Romanescu, T. R. Galeev, Z. A. Piazza, A. I. Boldyrev and L. S. Wang, *J. Am. Chem. Soc.*, 2012, **134**, 165–168.
- 20 C. Romanescu, T. R. Galeev, W. L. Li, A. I. Boldyrev and L. S. Wang, *Acc. Chem. Res.*, 2013, **46**, 350–358.
- 21 X. Wu, L. L. Zhao, J. Y. Jin, S. D. Pan, W. Li, X. Y. Jin, G. J. Wang, M. F. Zhou and G. Frenking, *Science*, 2018, **361**, 912–916.
- 22 H.-R. Li, X.-Q. Lu, Y.-Y. Ma, Y.-W. Mu, H.-G. Lu, Y.-B. Wu and S.-D. Li, *J. Clust. Sci.*, 2019, **30**, 621–626.
- 23 J. A. Dean, *Lange's handbook of Chemistry*, McGraw-Hill Book Co., 15th edn, 1999.
- 24 X. Chen, Y.-F. Zhao, Y.-Y. Zhang and J. Li, *J. Comput. Chem.*, 2019, **40**, 1105–1112.
- 25 D. J. Wales and H. A. Scheraga, *Science*, 1999, **285**, 1368–1372.
- 26 J. P. Perdew, K. Burke and M. Ernzerhof, *Phys. Rev. Lett.*, 1996, **77**, 3865.
- 27 J. VandeVondele, M. Krack, F. Mohamed, M. Parrinello, T. Chassaing and J. Hutter, *Comput. Phys. Commun.*, 2005, **167**, 103–128.
- 28 Y. Zhao and D. G. Truhlar, *Theor. Chem. Acc.*, 2008, **120**, 215–241.
- 29 J.-D. Chai and M. Head-Gordon, *Phys. Chem. Chem. Phys.*, 2008, **10**, 6615.



30 D. Feller, *J. Comput. Chem.*, 1996, **17**, 1571–1586.

31 L. Schuchardt, B. T. Didier, T. Elsethagen, L. Sun, V. Gurumoorthi, J. Chase, J. Li and T. L. Windus, *J. Chem. Inf. Model.*, 2007, **47**, 1045–1052.

32 M. J. Frisch, *Gaussian 16, Revision A.03*, Gaussian Inc., Wallingford, CT, 2016.

33 E. D. Glendening, C. R. Landis and F. Weinhold, *J. Comput. Chem.*, 2019, **40**, 2234–2241.

34 T. Ziegler and A. Rauk, *Theor. Chim. Acta*, 1977, **46**, 1–10.

35 M. Mitoraj and A. Michalak, *Organometallics*, 2007, **26**, 6576–6580.

36 M. P. Mitoraj, A. Michalak and T. Ziegler, *J. Chem. Theory Comput.*, 2009, **5**, 962–975.

37 G. te Velde, F. M. Bickelhaupt, E. J. Baerends, C. Fonseca Guerra, S. J. A. van Gisbergen, J. G. Snijders and T. Ziegler, *J. Comput. Chem.*, 2001, **22**, 931–967.

38 E. Van Lenthe and E. J. Baerends, *J. Comput. Chem.*, 2003, **24**, 1142–1156.

39 E. van Lenthe, E. J. Baerends and J. G. Snijders, *J. Chem. Phys.*, 1993, **99**, 4597.

40 D. Y. Zubarev and A. I. Boldyrev, *Phys. Chem. Chem. Phys.*, 2008, **10**, 5207–5217.

41 N. V. Tkachenko and A. I. Boldyrev, *Phys. Chem. Chem. Phys.*, 2019, **21**, 9590–9596.

42 W. Humphrey, A. Dalke and K. Schulten, *J. Mol. Graph.*, 1996, **14**, 33–38.

43 S. Klod and E. Kleinpeter, *J. Chem. Soc., Perkin Trans.*, 2001, **2**, 1893–1898.

44 E. Kleinpeter, S. Klod and A. Koch, *J. Mol. Struct.*, 2007, **811**, 45–60.

45 H. L. Schmider and A. D. Becke, *J. Mol. Struct. (THEOCHEM)*, 2000, **527**, 51–61.

46 T. Lu and F. Chen, *J. Comput. Chem.*, 2012, **33**, 580–592.

47 D. Geuenich, K. Hess, F. Köhler and R. Herges, *Chem. Rev.*, 2005, **105**, 3758–3772.

48 Povray, *Persistence of vision raytracer*, POV-Ray 3.7, <https://www.povray.org/>.

